CHEMISTRY OF MATERIALS

Article

pubs.acs.org/cm

Luminescent $CuInS_2$ Quantum Dots by Partial Cation Exchange in $Cu_{2-x}S$ Nanocrystals

Ward van der Stam,[†] Anne C. Berends,[†] Freddy T. Rabouw,[†] Tom Willhammar,[‡] Xiaoxing Ke,[‡] Johannes D. Meeldijk,[§] Sara Bals,[‡] and Celso de Mello Donega*[,†]

[†]Condensed Matter and Interfaces, Debye Institute for Nanomaterials Science, Utrecht University, Princetonplein 5, 3584 CC Utrecht, The Netherlands

[‡]Electron Microscopy for Materials Science (EMAT), University of Antwerp, Groenenborgerlaan 171, B-2020 Antwerp, Belgium

[§]Electron Microscopy Utrecht, Debye Institute for Nanomaterials Science, Utrecht University, 3584 CH Utrecht, The Netherlands

Supporting Information

ABSTRACT: Here, we show successful partial cation exchange reactions in $Cu_{2-x}S$ nanocrystals (NCs) yielding luminescent $CuInS_2$ (CIS) NCs. Our approach of mild reaction conditions ensures slow Cu extraction rates, which results in a balance with the slow In incorporation rate. With this method, we obtain CIS NCs with photoluminescence (PL) far in the near-infrared (NIR), which cannot be directly synthesized by currently available synthesis protocols. We discuss the factors that favor partial, self-limited cation exchange from $Cu_{2-x}S$ to CIS NCs, rather than complete cation exchange to In_2S_3. The product CIS NCs have the wurtzite crystal structure, which is understood in terms of conservation of the hexagonal close packing of the anionic sublattice of the parent NCs into the product NCs. These results are an important step toward the design of CIS NCs with sizes and shapes that are not attainable by direct synthesis protocols and may thus impact a number of potential applications.

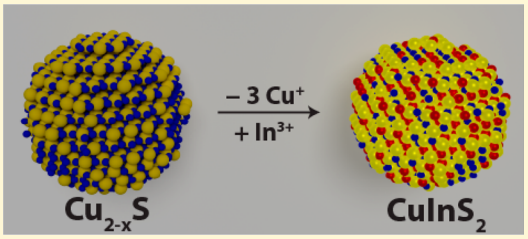

INTRODUCTION

Colloidal semiconductor nanocrystals (NCs) have attracted increasing attention due to their exciting and tunable optical properties, which render them promising materials for several applications.[1−4] For example, NCs can be used as luminescent probes for *in vivo* bioimaging[5,6] and light converters in displays and LEDs.[7,8] However, the presence of heavy metals such as cadmium and lead is an increasing concern, which limits the applicability of colloidal NCs.[8,9]

Copper indium dichalcogenide ($CuInE_2$, with E = S and/or Se) NCs have optical properties that can be tuned in the visible to the near-infrared (NIR; potentially up to 855 nm for $CuInS_2$ (CIS) and up to 1215 nm for $CuInSe_2$, (CISe)) spectral range, which makes them promising alternatives for the well-known heavy metal based NCs (CdE and PbE, with E = S, Se, Te).[10−14] For example, the direct bandgap of 1.45 eV and large absorption coefficients make CIS a suitable alternative absorber material for quantum dot and thin film photovoltaics (PV).[15−17] Additionally, the small self-absorption cross-section[10] makes CIS NCs very interesting materials as luminophores in luminescent solar concentrators.[18,19]

However, the currently available protocols for the direct colloidal synthesis of luminescent ternary NCs such as CIS and CISe produce only small quasi-spherical NCs.[10−12] Larger and anisotropic NCs with a homogeneous composition are difficult to obtain because multiple precursor reactivities need to be balanced for simultaneous thermolysis of the cationic precursors.[20] Otherwise, it is favorable for the reaction system to form instead binary NCs, such as $Cu_{2-x}S$.[21] Pure phase luminescent quasi-spherical CIS NCs have only been obtained with photoluminescence (PL) peak between 550 and 820 nm,[22−24] whereas large nonluminescent CIS nanorods are obtained when $Cu_{2-x}S$ NCs are used *in situ* as nucleation seeds.[25] Hence, there is a wide range of sizes and shapes that have not yet been explored for CIS NCs.

Here, we present a synthetic pathway toward ternary $CuInS_2$ NCs from binary $Cu_{2-x}S$ parent NCs by exploiting cation exchange (CE) reactions.[26−30] Nonluminescent $Cu_{2-x}S$ NCs are converted into luminescent CIS NCs, where the PL peak position of the product CIS NCs is determined by the size of the parent $Cu_{2-x}S$ NCs. This method allows us to synthesize CIS NCs with PL in the near-infrared (NIR) centered at 870 nm, which are not attainable in a direct fashion. Since colloidal $Cu_{2-x}S$ NCs can be synthesized with large control over size and shape (*e.g.*, nearly spherical NCs, hexagonal bipyramids, bifrustums and nanoplatelets, and ultrathin nanosheets),[30−34] the method described in this work may provide a pathway to prepare colloidal CIS NCs of as yet unexplored morphologies and functionalities.

Received: November 25, 2014
Revised: December 23, 2014
Published: December 29, 2014

DOI: 10.1021/cm504340h
Chem. Mater. 2015, 27, 621−628

EXPERIMENTAL SECTION

Materials. Copper (I) acetate (CuOAc, 97%), copper sulfate pentahydrate ($CuSO_4 \cdot 5H_2O$, ≥98%), copper (I) iodide (CuI, 99.99%), indium nitrate hydrate ($In(NO_3)_3 \cdot H_2O$, 99.99%), indium acetate ($InAc_3$, 99.99%), 1-dodecanethiol (DDT, ≥98%), 1-octadecene (ODE, 90%), trioctyl phosphine oxide (TOPO, 99%), trioctyl phosphine (TOP, 90%), oleic acid (OA, 90%), anhydrous toluene, methanol, and butanol were purchased from Sigma-Aldrich. ODE and TOPO were degassed prior to synthesis, all other materials were used as received.

Synthesis of 2.5 nm $Cu_{2-x}S$ NCs. The $Cu_{2-x}S$ NCs (size: 2.5 nm) were synthesized according to the method described by Wang et al.[34] In a round-bottom flask, 0.3 mmol of CuOAc and 1.1 g of TOPO were dissolved in 25 mL of previously degassed ODE. After additional degassing for 1 h at 100 °C the reaction mixture was further heated to 160 °C, and 1 mL of DDT was swiftly injected into the dark green solution under N_2 atmosphere. The NCs were allowed to grow for 90 min. Subsequently, the NCs were cooled to room temperature. They were washed by adding methanol and butanol (1:1 ratio), centrifugation at 3000 rpm for several minutes, and redispersion in 2 mL of toluene. This cycle was repeated 3 times.

Synthesis of 4 nm $Cu_{2-x}S$ NCs. For the synthesis of 4 nm sized $Cu_{2-x}S$ NCs the same procedure described above was followed, but the NCs were allowed to grow for an additional 2 h (total growth time; 3.5 h). The same washing steps were performed.

Synthesis of 11 nm $Cu_{2-x}S$ NCs. The 11 nm sized $Cu_{2-x}S$ NCs were synthesized according to an adaptation of the method described by Lu et al.[25] In a round-bottom flask, 0.8 mmol of $CuSO_4 \cdot 5H_2O$ (203 mg), 7.5 mL of DDT, and 6 mL of OA were mixed and gradually heated to 200 °C. Total heating time was 15 min, after which the solution was maintained at 200 °C for 2 h. The crude reaction mixture was purified in the same way as described above and redispersed in ∼5 mL of toluene.

Cation Exchange (CE) Reactions of Cu^+ for In^{3+} in $Cu_{2-x}S$ NCs. The cation exchange reactions were performed according to an adaptation of the method described by Son et al. for Cd^{2+} for Ag^+ exchange reactions.[27] One milliliter of a solution of $Cu_{2-x}S$ NCs ($\sim 10^{-8}$ M) in toluene was diluted three times, and 0.14 mmol of $In(NO_3)_3 \cdot H_2O$ dissolved in 1 mL of methanol was added. The In/Cu molar ratio in the reaction mixtures was ∼1 for all NC sizes. This ratio is a lower limit estimate since it assumes a 100% yield and no purification losses in the synthesis of the $Cu_{2-x}S$ NCs. Finally, 100 μL of TOP was added as Cu-extracting ligand, and the resulting solution was stirred for several days. The product NCs were thoroughly washed to remove excess precursor and ligands by adding methanol and butanol (1:1 ratio) and centrifugation at 3000 rpm for several minutes. Subsequently, the product NCs were dispersed in 2 mL of toluene.

Direct synthesis of 2.5 nm $CuInS_2$ NCs. For comparison, CIS NCs were directly synthesized following the method described by Li et al.[35] In a round-bottom flask, 0.4 mmol of CuI, 0.4 mmol of $InAc_3$, and 5 mL of DDT were mixed and degassed under vacuum at 100 °C for 1 h. Subsequently, the temperature was raised to 230 °C, and the NCs were allowed to grow for 11 min. The solution was cooled to room temperature, and the NCs were precipitated by addition of a methanol/butanol solution and centrifugation at 3000 rpm. The supernatant was discarded and the NCs were redispersed in toluene. The washing steps were repeated twice.

Optical Spectroscopy. Samples for optical measurements were prepared by diluting the washed NCs in anhydrous toluene under nitrogen and stored in sealed cuvettes. Absorption spectra were measured on a double beam PerkinElmer Lambda 16 UV−vis spectrometer. PL and PL excitation spectra were recorded by an Edinburgh Instruments FLS920 Spectrofluorimeter equipped with a 450 W xenon lamp as excitation source and double grating monochromators. PL decay curves were obtained by time-correlated single-photon counting via time-to-amplitude conversion. A pulsed diode laser (EPL-445 Edinburgh Instruments, 441 nm, 55 ps pulse width, 0.2−0.5 MHz repetition rate) was used as the excitation source.

Photoluminescence Quantum Yields. Photoluminescence (PL) quantum yields (QY) were measured using an integrating sphere mounted in an Edinburgh Instruments spectrofluorimeter equipped with double-grating excitation and emission monochromators, and a 450 W Xe lamp as the excitation source.[18] To avoid losses due to light scattering and reabsorption only sufficiently diluted (sub-micromolar concentration range) NC solutions were used. The intensity of the excitation light (400 nm) was measured after passing the sample and after passing the solvent (toluene) only. After correcting the recorded spectra for the sensitivity of the detector, the difference of the two intensities was attributed to absorption. The emission spectra were measured under the same conditions as the absorption but detected over a broader spectral region starting at a wavelength 5 nm longer than that used for excitation (i.e., 405 nm). The emission spectra were recorded for the excited sample solution and for the solvent only and subsequently corrected for the instrumental response. The PL QYs were obtained by dividing the integrated emission intensities by the integrated absorption intensities. Because of the instrumental limitations, PL QYs can be measured only up to ∼850 nm.

Transmission Electron Microscopy. Transmission electron microscopy (TEM) and energy dispersive X-ray spectroscopy (EDS) were performed using a FEI Tecnai-12 microscope operating at 120 kV and a FEI Tecnai-20F microscope operating at 200 kV. Samples for TEM imaging were prepared by drop-casting a toluene solution of NCs onto a carbon-coated copper (400-mesh) TEM grid. The excess liquid was removed by blotting using filter paper.

Energy Dispersive X-ray Spectroscopy Mapping. Scanning TEM EDS measurements were performed on a FEI Tecnai-20F microscope operating at 200 kV. EDS measurements were performed using a dedicated low background holder and Cu-free Ni TEM grids. Acquisition time for EDS measurements was ∼30 s to ∼1 min. The EDS signal was acquired with an EDAX Si(Li) detector and processed in Tecnai Imaging and Analysis software (TIA), using the following lines: S−K at 2.3 keV, In−L at 3.3 keV, and Cu−K at 8.0 keV. The S−K and In−L are well resolved, but Cu−K is partially overlapping with the Ni−Kβ peak at 8.26 keV (originating from the nickel grid). The software deconvoluted these two peaks. The automatically acquired background subtraction was adjusted manually where necessary in order to quantitatively deconvolute the peaks and no thickness or ZAF corrections were applied. To ensure that the elemental concentrations were statistically valid and representative of the whole NC ensemble, EDS analyses were performed on wide areas (10^4−10^5 nm^2), encompassing several thousands of NCs. We note here that even when taking the usual precautions (dedicated low background holder and Cu-free Ni TEM grids), there is always a background Cu signal contributing to the EDS spectrum. We estimated the uncertainty in the composition of the NCs by averaging values obtained for different samples. Since the elemental ratios are defined with respect to S, standard deviation values are not provided for the S ratios.

High-Resolution Scanning Transmission Electron Microscopy (HRSTEM). High-resolution scanning transmission electron microscopy (HRSTEM) images of the CIS NCs were acquired using an FEI Titan^3 operated at an accelerating voltage of 120 kV. The images were collected using a high angle annular dark field (HAADF) detector. The samples were prepared by adding a droplet of the toluene dispersion to a carbon coated copper grid. The lattice averaging was performed by calculating a fast Fourier transform (FFT) from the area of interest, extracting one Fourier component from each of the lattice points of the FFT, and performing an inverse Fourier transform to create the final map. The image processing was performed using the software CRISP.[36]

X-ray Diffractometry. X-ray diffraction (XRD) measurements were performed with a Bruker D2 Phaser, equipped with a Co Kα X-ray source with X-ray wavelength of 1.79026 Å. Thin solid film NC samples for XRD were prepared by drop-casting a concentrated NC solution in chloroform on a Si wafer and evaporating the solvent.

DOI: 10.1021/cm504340h
Chem. Mater. 2015, 27, 621−628

RESULTS AND DISCUSSION

Luminescent 2.5 nm CIS NCs by Partial Cation Exchange in Cu_{2-x} NCs. Nonluminescent 2.5 nm $Cu_{2-x}S$ nanocrystals (NCs), with a first absorption transition around 500 nm (dashed line in Figure 1a), are converted into NCs that show efficient photoluminescence (PL) both in the visible (peak at 650 nm) and in the NIR (peak at 900 nm, solid line in Figure 1a). The position of the higher energy PL peak is in close agreement with that observed for directly synthesized $CuInS_2$ (CIS) NCs of 2.5 nm (viz., 665 nm). Further, PL lifetime measurements on the CIS NCs obtained by cation exchange (CE), while monitoring the higher energy PL peak (Figure 1b), yields lifetime values of τ_1 = 36 ns and τ_2 = 206 ns, which are comparable to those obtained on directly synthesized CIS NCs of comparable size and shape (τ_1 = 26 ns and τ_2 = 205 ns; Supporting Information Figure S1). Hence, the recombination pathways in the product CIS NCs obtained by CE in $Cu_{2-x}S$ NCs are essentially the same as those in CIS NCs synthesized by direct methods. This also indicates that the PL QYs of the CIS NCs obtained by CE reactions are comparable to those of the directly synthesized CIS NCs, which are in the 5 to 10% range, depending on the sample. We note that these PL QYs are comparable to the highest values reported in the literature for CIS NCs.[11,37] Higher PL QYs (as high as 85%) have been reported only for CIS/CdS and CIS/ZnS core/shell or graded alloy NCs.[11,35,38]

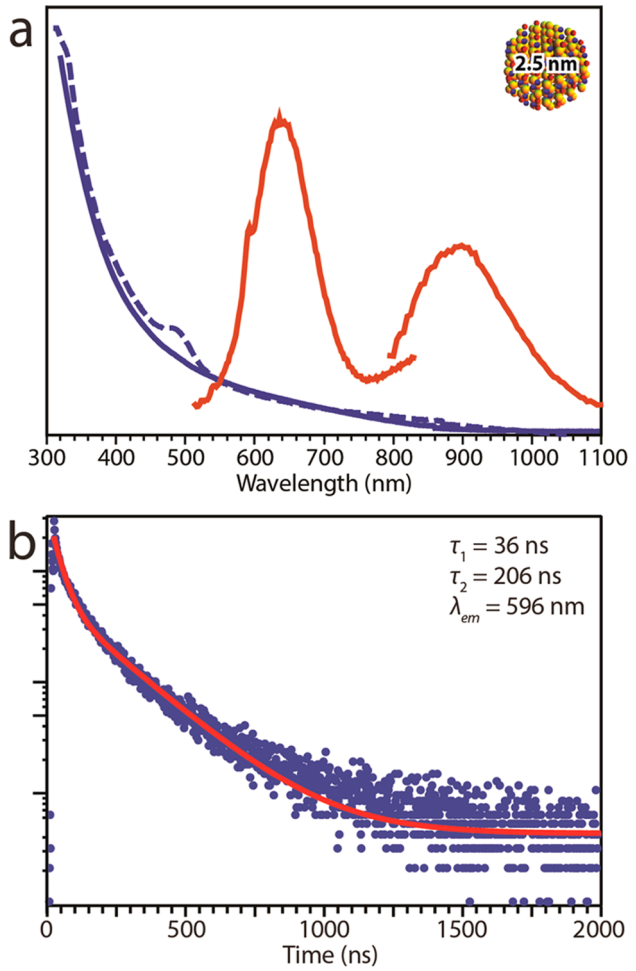

Figure 1. (a) Absorption and photoluminescence (PL) spectra of 2.5 nm CIS NCs obtained by partial cation exchange in $Cu_{2-x}S$ NCs (blue and red solid lines). Two PL spectra are plotted due to the change of detector necessary to obtain a good signal in the NIR region. The absorption spectrum of the parent 2.5 nm $Cu_{2-x}S$ NCs is also shown (blue dashed line). (b) PL decay curve of CIS NCs (2.5 nm) obtained by partial CE reaction while monitoring the higher energy PL. Fitting a biexponential to the data (red curve) yields a fast component with τ_1 = 36 ns and a slow component with τ_2 = 206 ns. The decay curve obtained while monitoring the lower energy PL peak is shown in the Supporting Information (Figure S2).

CIS NCs typically exhibit a single broad PL band located several hundred meV below the apparent absorption edge, which is usually ascribed to donor−acceptor pair (DAP) recombination, by analogy to bulk CIS.[11,23] This explains the large global Stokes shift and relatively slow decay dynamics.[23] The observation of two bands in the PL spectrum of the 2.5 nm CIS NCs obtained by CE (Figure 1a) is thus remarkable. As discussed above, the higher energy peak can be ascribed to DAP recombination pathways that are essentially the same as those present in directly synthesized CIS NCs. In contrast, the PL lifetime measured while monitoring the lower energy band is much longer than that observed in similar sized CIS NCs obtained by direct synthesis (*viz.*, τ_1 = 42 ns and τ_2 = 501 ns, Supporting Information Figure S2). This is consistent with exciton recombination involving more localized states, such as those associated with surface and/or internal defects. Considering the large surface/volume ratio of such small NCs and the fact that CE is essentially a surface process (see mechanism section below), it is likely that part of the CIS NC ensemble contains surface defects that give rise to additional recombination pathways. The limited resolution of the FEI Tecnai-12 TEM for particles smaller than 3 nm did not allow us to clearly visualize the 2.5 nm NCs. The formation of CIS NCs by partial cation exchange in $Cu_{2-x}S$ NCs (2.5 nm diameter) is, however, confirmed by energy dispersive X-ray spectroscopy (EDS, Supporting Information Figure S3), which reveals a Cu/In/S ratio of 1.0 ± 0.12:1.4 ± 0.16:2. It is noteworthy that this ratio is consistent with the observed optical properties since the highest PL QYs are typically associated with In-rich (or Cu-poor) CIS NCs.[11,37]

Luminescent 4 nm CIS NCs by Partial Cation Exchange in $Cu_{2-x}S$ NCs. The partial CE reaction was also exploited to convert larger $Cu_{2-x}S$ parent NCs (4 nm) into CIS NCs. In this case, the product NCs show a single PL peak at 870 nm (Figure 2a). This clearly demonstrates that the NC size is inherited from the parent $Cu_{2-x}S$ NCs since this emission wavelength is consistent with CIS NCs of 4 nm in diameter. Considering that the optical properties are determined by the size of the CIS NCs, we can conclude that the method presented here provides a pathway to synthesize CIS NCs with efficient PL in the NIR, which have not yet been synthesized by direct synthesis protocols. Compared to the smaller NCs (2.5 nm), quantum confinement is relaxed leading to PL at lower energies.

The PL decay of these larger (*viz.*, 4 nm) CIS NCs can be well described by a biexponential fit, with a fast component τ_1 = 68 ns and slow component τ_2 = 408 ns (Figure 2b). These decay constants are slower than those usually observed in small CIS NCs. This difference is qualitatively explained by Fermi's golden rule,[39] according to which the spontaneous emission rate scales with the transition energy. More precisely, for excitonic transitions in NCs of varying sizes the radiative lifetime should scale linearly with the emission wavelength.[40] The difference between the PL lifetimes of the two sizes of CIS

DOI: 10.1021/cm504340h
Chem. Mater. 2015, 27, 621−628

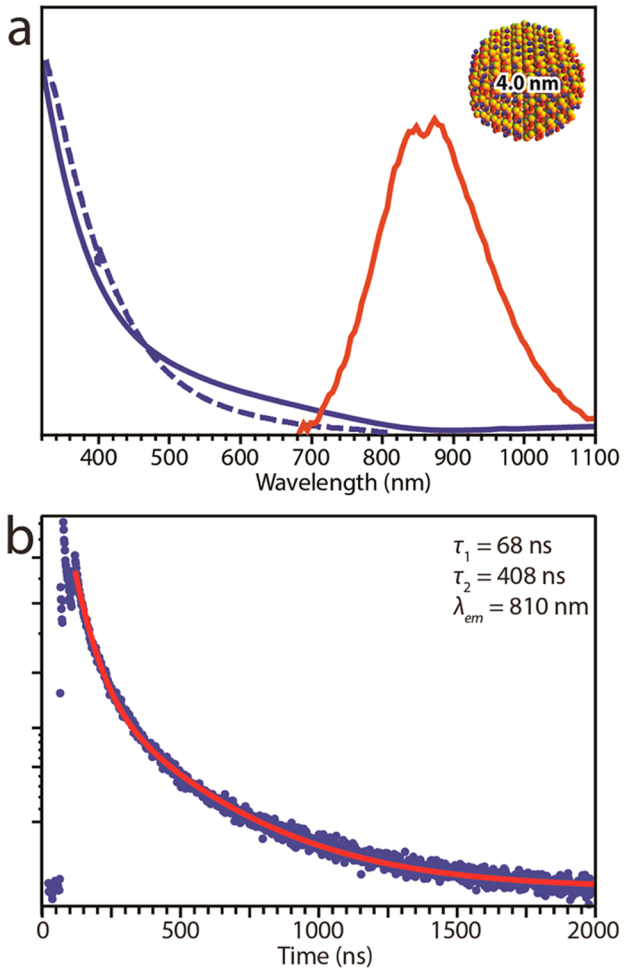

Figure 2. (a) Absorption and photoluminescence (PL) spectra of CIS NCs obtained by partial cation exchange in 4 nm diameter $Cu_{2-x}S$ NCs (blue and red full lines). The absorption spectrum of the parent $Cu_{2-x}S$ NCs is also shown (blue dotted line). (b) PL decay of 4 nm diameter CIS NCs obtained from $Cu_{2-x}S$ NCs by CE reactions. Fitting a biexponential to the data (red curve) yields a fast component with τ_1 = 68 ns and a slow component with τ_2 = 408 ns.

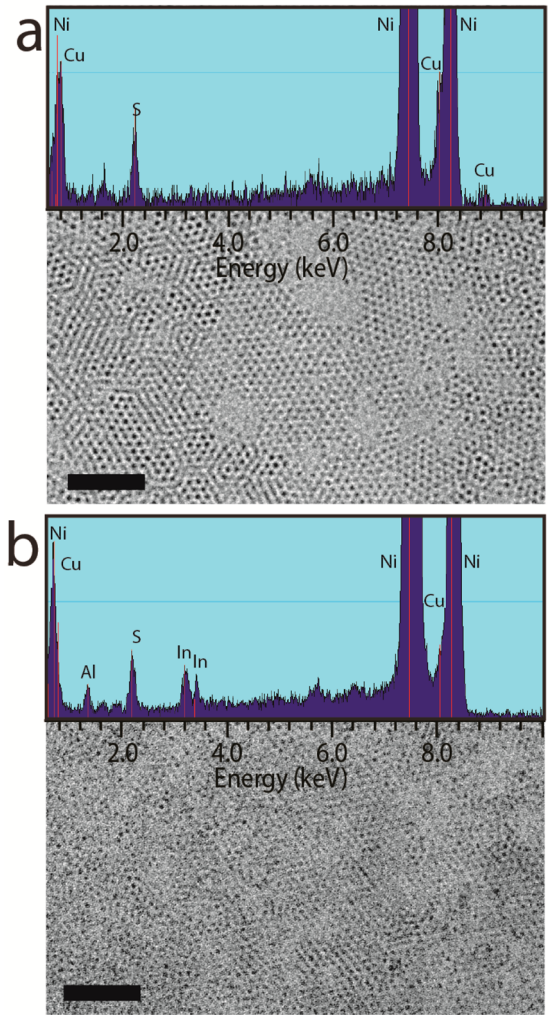

Figure 3. (a) Transmission electron microscopy (TEM) image of 4 nm $Cu_{2-x}S$ parent NCs. Inset displays the EDS spectrum of the $Cu_{2-x}S$ parent NCs. (b) TEM image of 4 nm CIS NCs, obtained from $Cu_{2-x}S$ NCs by partial CE. Inset displays the EDS spectrum of the CIS NCs. Scale bars correspond to 50 nm.

NCs investigated here is, however, larger than predicted by Fermi's golden rule (emission wavelength ratio is 1.3, while the lifetime ratio is 1.9). This indicates that the emission transitions in CIS NCs are not excitonic in nature but instead involve DAP recombination,[23] in agreement with the assignment presented above for the smaller NCs. Although the PL QYs of the larger CIS NCs could not be directly determined due to limitations of our setup in the NIR, the similarity of the PL decay curves suggests that they are at least of the same order of magnitude as those observed for the smaller NCs since pronounced PL quenching should result in faster decays due to increased nonradiative recombination rates.

TEM measurements revealed that the size of the parent $Cu_{2-x}S$ NCs is preserved in the product CIS NCs (Figure 3). The product NCs no longer form self-assembled superstructures on the TEM grid, suggesting that the size dispersion has slightly increased. It is also possible that the NC self-assembly is prevented by the presence of reaction byproducts that were not completely removed by the washing procedure. The successful transformation of the parent $Cu_{2-x}S$ NCs into product CIS NCs is clearly reflected in EDS measurements, where In peaks around 3.2 keV are observed in the product NCs (Figure 3b). Quantification of the EDS measurements gives a Cu/S ratio of 2 ± 0.16:1 for the parent $Cu_{2-x}S$ NCs (Figure 3a) and a Cu/In/S ratio of 1.1 ± 0.14:1.6 ± 0.21:2 for the product CIS NCs (Figure 3b). It should be noted that this Cu/In ratio is consistent with the observation of efficient PL,[11,37] in line with the results obtained for the smaller NCs.

X-ray diffraction (XRD) measurements (Supporting Information, Figure S4) suggest that the In^{3+} for Cu^{+} cation exchange in $Cu_{2-x}S$ NCs is accompanied by a crystal structure transformation from low-chalcocite $Cu_{2-x}S$ to wurtzite CIS. The peaks are, however, severely broadened due to finite size effects, precluding a definite assignment of the observed reflections. Nevertheless, the formation of pure phase wurtzite CIS is unambiguously confirmed by high-resolution scanning transmission electron microscopy (HRSTEM) measurements (Figure 4). The 4 nm CIS product NCs were imaged along two crystallographic directions, *viz.* [100] and [101]. The images reveal the expected atomic arrangement for wurtzite CIS NCs. In Figure 4a, the NC viewed along the [100] direction is indicated by the red circle, whereas the NC viewed along the [101] direction is indicated by the blue circle. In the other panels, the same colors are used for the two directions, red for

DOI: 10.1021/cm504340h
Chem. Mater. 2015, 27, 621−628

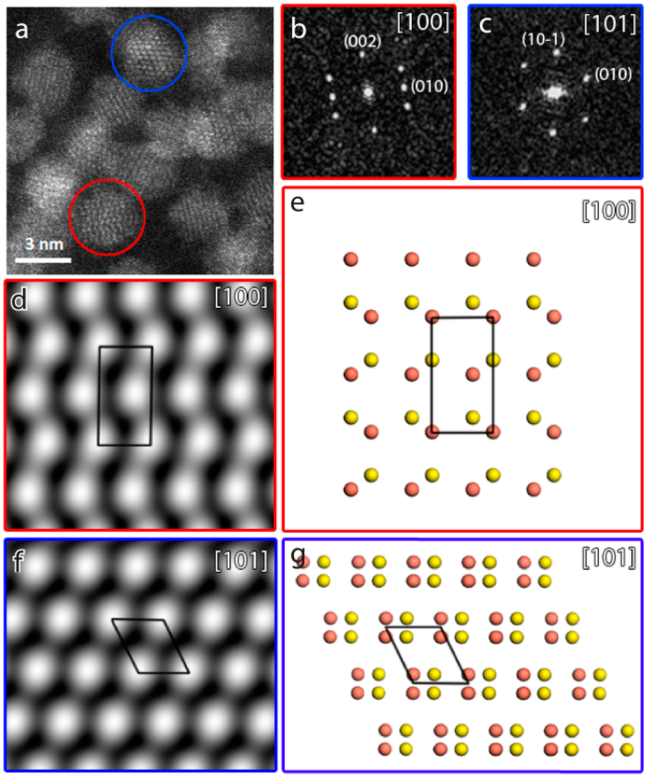

Figure 4. (a) High-resolution scanning transmission electron microscopy (HRSTEM) image of the 4 nm product CIS NCs viewed along the [100] direction with respect to the electron beam (red circle) and along the [101] direction (blue circle). (b,c) Calculated FFTs from the areas indicated by the red circle (b) and by the blue circle (c). (d) Lattice averaged image from the red area in panel a reveal the atomic arrangement along the [100] direction. (e) The atomic arrangement fits well with the wurtzite CIS crystal structure. (f) Lattice averaged image of the blue area in panel a shows the atomic arrangement along the [101] direction. (g) The atomic arrangement fits well with the wurtzite CIS crystal structure. The yellow spheres denote the sulfur atoms and the orange spheres denote the Cu/In atoms in panels e and g.

[100] (Figure 4b,d,e) and blue for [101] (Figure 4c,f,g). When fast Fourier transformation (FFT) is calculated from the circled areas, the characteristic lattice of wurtzite CIS is directly evident in both cases (Figure 4b,c). When the images of the NCs from panel a are lattice averaged, clear atomic positions are obtained (Figure 4d,f). The observed atomic arrangement fits well with the wurtzite CIS crystal structure in both directions, as can be seen in the models depicted in Figure 4e,g, confirming the wurtzite crystal structure of the product 4 nm CIS NCs. Note that the contrast of the HAADF-STEM images is related to the atomic number so the contribution of In and Cu will dominate over S. The resolution of the HRSTEM images is less than 3 Å, which further prevents resolving the S atoms from the Cu/In atoms. The low resolution is due to poor beam stability of the material and severe contamination.

CIS NCs by Partial Cation Exchange in 11 nm $Cu_{2-x}S$ NCs. To demonstrate that the method developed in this work can also yield CIS NCs of unprecedented sizes, we performed CE in $Cu_{2-x}S$ NCs of 11 nm. Although the product CIS NCs are nonluminescent due to their large size, the outcome of the CE reaction is more easily analyzed with TEM and XRD. The UV–vis absorption spectrum of the product NCs shows an absorption onset that is close to the bulk bandgap of CIS (1.4 eV, Figure 5a). It is also interesting to note that the NIR plasmon band associated with Cu vacancies in $Cu_{2-x}S$ NCs

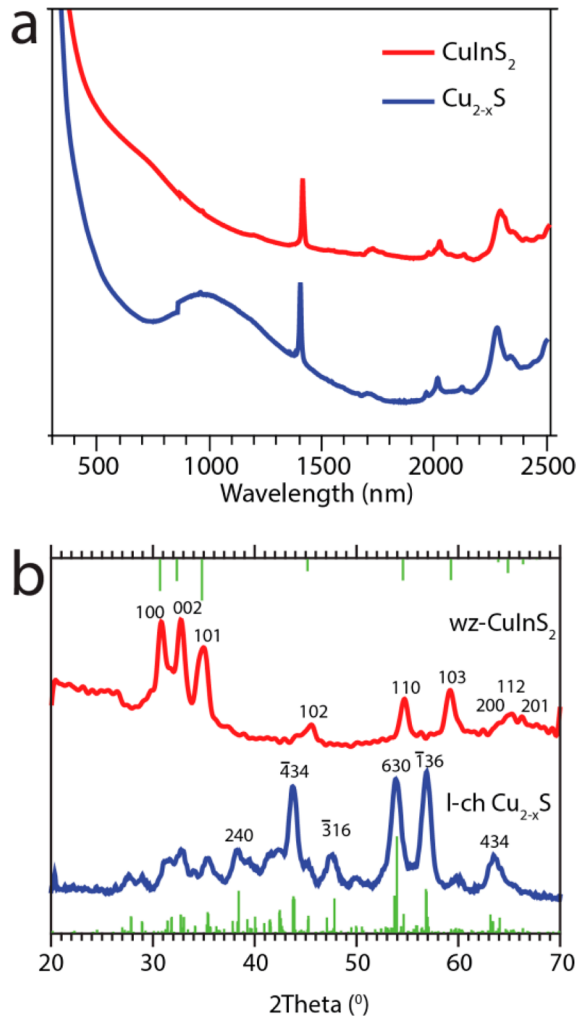

Figure 5. (a) Absorption spectrum of 11 nm CIS NCs obtained by cation exchange from $Cu_{2-x}S$ NCs (red line). The absorption spectrum of the parent 11 nm $Cu_{2-x}S$ NCs is also shown (blue line). (b) XRD patterns (Co Kα source) of 11 nm CIS NCs obtained by cation exchange from $Cu_{2-x}S$ NCs (wurtzite, wz, red line) and of the parent $Cu_{2-x}S$ NCs (low-chalcocite, l-ch, blue line). Reference bars (green lines) are from JCPDS PDF-card 01-077-9459 for wurtzite CIS and R120113-9 for low-chalcocite.[41]

disappeared after the CE. Moreover, XRD measurements reveal a clear transition from the hexagonal low-chalcocite $Cu_{2-x}S$ crystal structure to the hexagonal wurtzite CIS crystal structure (Figure 5b), consistent with the observations discussed above for the 4 nm CIS NCs. The structural change is also clear in the electron diffraction patterns (Supporting Information, Figure S5). However, the size dispersion of the product CIS NCs is much larger than that of the parent $Cu_{2-x}S$ NCs (Supporting Information, Figure S5), suggesting that in this case CE was accompanied by partial dissolution and ripening. As will be discussed below, this indicates that there was a slight imbalance between the Cu^{+} outgoing and the In^{3+} incoming rates.

Mechanism. Cation exchange reactions consist of a chain of inherently linked elementary kinetic steps, which must proceed in a concerted manner.[26,42] The driving force for the reaction is determined by the energy balance of the overall reaction and

DOI: 10.1021/cm504340h
Chem. Mater. 2015, 27, 621–628

therefore depends on the relative stabilities of the incoming and outgoing cations in solution and in the NC. It should also be noted that the cation exchange would not proceed beyond the surface in the absence of solid state diffusion fluxes in the NC,[43] allowing the native cations to diffuse outward and the new cations to diffuse inward. The overall energy balance is thus also strongly dependent on the activation energies for diffusion of both the incoming and outgoing cations in the NC.

Figure 6 schematically depicts the elementary steps that can be identified in the Cu^+ for In^{3+} exchange in $Cu_{2-x}S$ NCs. It is

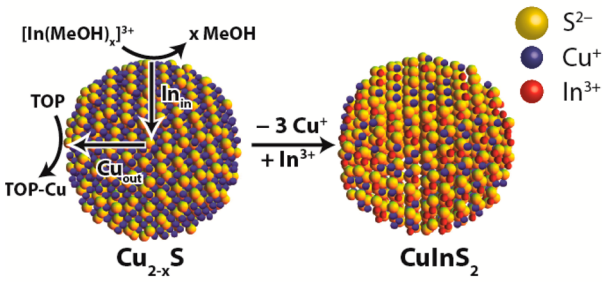

Figure 6. Schematic illustration of the elementary kinetic steps involved in conversion of $Cu_{2-x}S$ NCs into $CuInS_2$ NCs by Cu^+ for In^{3+} cation exchange. Cu^+ extraction (mediated by trioctylphosphine, TOP) and In^{3+} incorporation into Cu^+ vacancies take place at the NC surface and set in motion two solid state cation diffusion fluxes (inward diffusion of In^{3+}, In_{in}, and outward diffusion of Cu^+, Cu_{out}).

interesting to note that the Cu^+ extraction and the In^{3+} incorporation proceed by separate chemical pathways, in contrast to other well-known nanoscale cation exchange reactions (*e.g.*, Cd^{2+} for Zn^{2+} exchange in ZnSe NCs using $Cd(oleate)_2$), in which the place exchange is mediated by a single ligand.[43] In the present case, Cu^+ (a soft Lewis acid with absolute hardness η = 6.28 eV)[44] is extracted from the $Cu_{2-x}S$ NCs by tryoctylphosphine (a soft Lewis base with $\eta \approx 6$ eV),[26] while In^{3+} (a hard Lewis acid with η = 13 eV)[44] is transported to the NC surface as a complex with the solvent molecules (methanol) and is subsequently incorporated in the Cu^+ vacancies. It should be noted that the off-stoichiometry of the parent $Cu_{2-x}S$ NCs is due to native Cu vacancies. These vacancies are not compensated by the formation of Cu^{2+} ions, but instead lead to free charge carriers (holes) in the valence band, effectively keeping the Cu atoms in the +1 valency and changing the valency of some S atoms from −2 to −1.[45] The free holes give rise to a localized plasmon resonance, which becomes stronger with decreasing Cu content (*i.e.*, increasing density of free holes).[45] Interestingly, the extraction of Cu atoms from the NCs by TOP does not increase the plasmon resonance, but rather causes its disappearance (see e.g., Figure 5a above). This is consistent with the fact that the Cu atoms are extracted as Cu^+, thereby removing also the excess holes since the CIS NCs obtained after the cation exchange are In^{3+}-rich. The removal of the excess holes by extraction of Cu^{2+} ions instead of Cu^+ is unlikely since the binding energies for TOP-Cu^{2+} are much smaller than those for TOP-Cu^+ (Cu^{2+} is a harder Lewis base, with η = 8.27 eV).[44]

As a consequence of the separate chemical pathways for Cu extraction and In incorporation, the extraction rate of the Cu^+ ions (Cu_{out}) and the incorporation rate of the In^{3+} ions (In_{in}) must be precisely balanced, otherwise the NCs will either dissolve (Cu_{out} faster than In_{in}) or the CE reaction will simply not proceed (Cu_{out} too slow). Several CE experiments were carried out with small variations in the reaction conditions (*i.e.*, higher temperatures of 50−100 °C, higher concentration, different CE precursors, and Cu-extracting ligands), but these conditions failed to effectively convert $Cu_{2-x}S$ NCs into CIS NCs because the Cu^+ extraction rate was too fast compared to the In^{3+} incorporation rate, resulting in dissolution of the NCs. This highlights the sensitivity of the cation exchange process toward external synthetic conditions.

CE reactions are very often topotactic, preserving the crystal structure of the parent NCs into the product NCs.[26−30] More precisely, the anionic sublattice is conserved, while the cations are exchanged. In this way, metastable crystal structures can be obtained, *e.g.*, wurtzite ZnS starting from $Cu_{2-x}S$.[28−30] The present case is special since partial CE is required in order to form the ternary CIS crystal structure rather than fully exchanged In_2S_3 (in principle, the In/Cu molar ratio of the CE reaction does allow full exchange to occur). This requires strict control over the incorporation and extraction rates of the cations. $Cu_{2-x}S$ exists in multiple crystal structures, determined by the anionic arrangement and the concentration of Cu vacancies indicated by x (*i.e.*, monoclinic low-chalcocite Cu_2S, djurleite $Cu_{1.96}S$, and roxbyite $Cu_{1.78}S$, as well as hexagonal low- and high-chalcocite Cu_2S, digenite $Cu_{1.8}S$, and covellite CuS).[46] A recent *in situ* X-ray study showed that small $Cu_{2-x}S$ NCs (diameter < 7 nm) typically have the near-stoichiometric hexagonal high-chalcocite structure.[47] Our XRD measurements reveal a low-chalcocite crystal structure for $Cu_{2-x}S$ particles of 11 nm in diameter (Figure 5b) and indicate a low-chalcocite crystal structure for 4 nm NCs (Figure S4, Supporting Information). The main difference between hexagonal low- and high-chalcocite is in the atomic positions of the Cu atoms, whereas the anions lie in a hexagonally close packed (hcp) arrangement in both cases.[41,48,49] Nanocrystalline CIS can attain two crystal structures, *viz.* roquesite and wurtzite. Roquesite is a zinc blende derivative where the sulfide anions are on a face centered cubic (fcc) sublattice, while wurtzite CIS is a hexagonal structure with an hcp anionic sublattice. CE reactions with djurleite and low- and high-chalcocite $Cu_{2-x}S$ NCs as parent NCs are expected to result in wurtzite products, due to the hexagonal symmetry of the starting crystal structure. Hence, in our CE reaction, wurtzite CIS NCs are favored over roquesite CIS since the transformation of $Cu_{2-x}S$ into the latter would require a substantial restructuring of the anionic sublattice.[41,50] This is also confirmed by XRD and HRSTEM measurements discussed above.

In_2S_3 exists in three crystal structures, denoted as α, β, and γ, where β-In_2S_3 is the stable structure up to 693 K.[51] All In_2S_3 crystal structures have an fcc stacking of S^{2-} anions, but differ in the ordering of the In^{3+} cations. Hence, the anion sublattice is intrinsically different from hexagonal $Cu_{2-x}S$ and wurtzite CIS, which is an important feature in avoiding full exchange from $Cu_{2-x}S$ into In_2S_3. Figure 7 compares the rearrangement of the anion sublattice required for the partial conversion of hexagonal low-chalcocite $Cu_{2-x}S$ into wurtzite CIS (Figure 7a) to the full conversion of hexagonal low-chalcocite $Cu_{2-x}S$ into β-In_2S_3 (Figure 7b). Low-chalcocite $Cu_{2-x}S$ and wurtzite CIS both have an hcp anion sublattice, with the hexagonal layers of S^{2-} anions ABAB stacked. This conversion requires a mere 1.4% contraction within the layers and 6.4% between the layers. The anions in β-In_2S_3, however, are ABC stacked. Hence, the conversion from low-chalcocite to β-In_2S_3 would require that four of every six anion layers shift over 58% of a S−S distance. Although such rearrangements from an hcp to an fcc anion

DOI: 10.1021/cm504340h
Chem. Mater. 2015, 27, 621−628

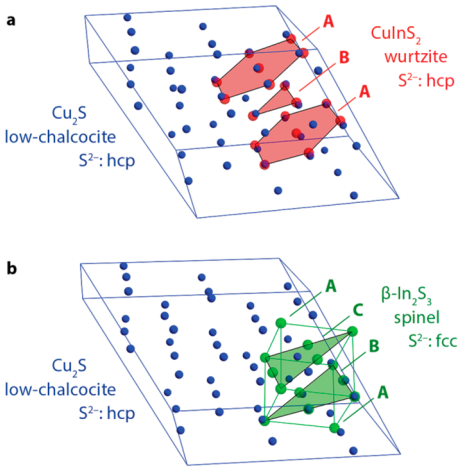

Figure 7. Comparison of the anionic sublattice of low-chalcocite $Cu_{2-x}S$ with wurtzite CIS, showing that the anionic sublattice of low-chalcocite $Cu_{2-x}S$ (blue spheres) is compatible with wurtzite CIS (red spheres) since both anionic sublattices have an hcp arrangement (a). Comparison of low-chalcocite unit cell (blue spheres) with In_2S_3 (green spheres). The spinel In_2S_3 structure has an fcc anionic sublattice, where layer C has to dislocate by 58% of a S−S distance in order to fit in the low-chalcocite lattice (b).

sublattice have been demonstrated before,[52] they have high activation barriers and require high reaction temperatures. Consequently, the low reaction temperatures employed in this work limit the CE to the extent that only partial exchange occurs, with luminescent ternary CIS as the final product.

CONCLUSIONS

We show successful partial, self-limited cation exchange (CE) reactions from binary low-chalcocite $Cu_{2-x}S$ NCs to luminescent ternary wurtzite $CuInS_2$ (CIS) NCs. With this method, large CIS NCs of 4 nm can be obtained with photoluminescence (PL) in the near-infrared (NIR), which is not possible by direct synthesis protocols. Slow extraction of Cu^+ is essential, due to the balance between the Cu extraction rate and the slow incorporation rate of In^{3+}. This slow Cu_{out} rate is achieved by choosing mild reaction temperatures. Furthermore, low reaction temperatures ensure that the CE is partial and prevent the formation of fully exchanged In_2S_3. The method presented here may prove beneficial for several applications where shape selective deposition techniques are used to fabricate assembled 2D layers, for example, in the field of photovoltaics or nanophotonics. The combination of multiple morphologies attainable for $Cu_{2-x}S$ NCs and the postsynthetic control over the composition toward CIS can thus result in the successful implementation of luminescent CIS NCs in several devices and in further tunability of the optoelectronic properties of CIS NCs. The problems arising from Cd-based luminescent NCs, such as toxicity, can be circumvented with this approach, which will prove beneficial for several applications in the field of photovoltaics, bioimaging, and lighting.

ASSOCIATED CONTENT

Supporting Information

Photoluminescence (PL) decay of directly synthesized 2.5 nm CIS NCs, near-infrared PL decay of 2.5 nm CIS NCs, energy dispersive X-ray spectroscopy (EDS) spectrum of 2.5 nm CIS NCs, X-ray diffraction measurements of 4 nm $Cu_{2-x}S$ and CIS NCs, transmission electron microscopy (TEM), electron diffraction (ED) measurements, and particle size histograms of large 11 nm $Cu_{2-x}S$ and CIS NCs. This material is available free of charge via the Internet at http://pubs.acs.org.

AUTHOR INFORMATION

Corresponding Author

*E-mail: c.demello-donega@uu.nl.

Author Contributions

The manuscript was written through contributions of all authors.

Notes

The authors declare no competing financial interest.

ACKNOWLEDGMENTS

W.v.d.S. and C.d.M.D. acknowledge financial support from the division of Chemical Sciences (CW) of The Netherlands Organization for Scientific Research (NWO) under grant number ECHO.712.012.001. S.B. and T.W. acknowledge financial support from European Research Council (ERC Starting Grant #335078-COLOURATOMS). The authors also appreciate financial support from the European Union under the Seventh Framework Program (Integrated Infrastructure Initiative No. 262348 European Soft Matter Infrastructure, ESMI). The authors thank Josine Bulle for the synthesis of 4 nm $Cu_{2-x}S$ NCs, Gang Wang for XRD measurements and Joost van der Lit for image processing assistance.

REFERENCES

(1) Rogach, A. L.; Talapin, D. V.; Shevchenko, E. V.; Kornowski, A.; Haase, M.; Weller, H. *Adv. Funct. Mater.* **2002**, *12*, 653−664.
(2) Donega, C. D. M. *Chem. Soc. Rev.* **2011**, *40*, 1512−1546.
(3) Skrabalak, S. E.; Xia, Y. *ACS Nano* **2009**, *3*, 10−15.
(4) Talapin, D. V.; Murray, C. B. *Science* **2005**, *310*, 86−89.
(5) Zhao, Y.; van Rooy, I.; Hak, S.; Fay, F.; Tang, J.; de Lange Davies, C.; Skobe, M.; Allen Fisher, E.; Radu, A.; Fayad, Z. A.; de Mello Donega, C.; Meijerink, A.; Mulder, W. J. M. *ACS Nano* **2013**, *7*, 10362−10370.
(6) Li, L.; Daou, T.; Texier, I.; Chi, T. K. *Chem. Mater.* **2009**, *21*, 2422−2429.
(7) Bourzac, K. *Nature* **2013**, *493*, 283.
(8) Shirasaki, Y.; Supran, G.; Bawendi, M.; Bulović, V. *Nat. Photonics* **2012**, *7*, 13−23.
(9) Zhang, Y.; Xie, C.; Su, H.; Liu, J.; Pickering, S.; Wang, Y.; Yu, W. W.; Wang, J.; Wang, Y.; Hahm, J.; Dellas, N.; Mohney, S. E.; Xu, J. *Nano Lett.* **2011**, *11*, 329−332.
(10) Kruszynska, M.; Borchert, H.; Parisi, J.; Kolny-Olesiak, J. *J. Am. Chem. Soc.* **2010**, *132*, 15976−15986.
(11) Kolny-Olesiak, J.; Weller, H. *ACS Appl. Mater. Interfaces* **2013**, *5*, 12221−12237.
(12) Yarema, O.; Bozyigit, D.; Rousseau, I.; Nowack, L.; Yarema, M.; Heiss, W.; Wood, V. *Chem. Mater.* **2013**, *25*, 3753−3757.
(13) Reifsnyder, D. C.; Ye, X.; Gordon, T. R.; Song, C.; Murray, C. B. *ACS Nano* **2013**, *7*, 4307−4315.
(14) Kim, S.; Kang, M.; Kim, S.; Heo, J.-H.; Noh, J. H.; Im, S. H.; Seok, S. I.; Kim, S.-W. *ACS Nano* **2013**, *7*, 4756−4763.
(15) Meillaud, F.; Shah, A.; Droz, C.; Vallat-Sauvain, E.; Miazza, C. *Sol. Energy Mater. Sol. Cells* **2006**, *90*, 2952−2959.
(16) Shockley, W.; Queisser, H. J. *J. Appl. Phys.* **1961**, *32*, 510.
(17) Panthani, M. G.; Stolle, C. J.; Reid, D. K.; Rhee, D. J.; Harvey, T. B.; Akhavan, V. A.; Yu, Y.; Korgel, B. A. *J. Phys. Chem. Lett.* **2013**, *4*, 2030−2034.
(18) Krumer, Z.; Pera, S. J.; van Dijk-Moes, R. J. A.; Zhao, Y.; de Brouwer, A. F. P.; Groeneveld, E.; van Sark, W. G. J. H. M.; Schropp,

DOI: 10.1021/cm504340h
Chem. Mater. 2015, 27, 621−628

R. E. I.; de Mello Donega, C. *Sol. Energy Mater. Sol. Cells* **2013**, *111*, 57−65.
(19) Erickson, C. S.; Bradshaw, L. R.; McDowall, S.; Gilbertson, J. D.; Gamelin, D. R.; Patrick, D. L. *ACS Nano* **2014**, *8*, 3461−3467.
(20) Tan, J. M. R.; Lee, Y. H.; Pedireddy, S.; Baikie, T.; Ling, X. Y.; Wong, L. H. *J. Am. Chem. Soc.* **2014**, *136*, 6684−6692.
(21) Kruszynska, M.; Borchert, H.; Parisi, J.; Kolny-Olesiak, J. *J. Nanoparticle Res.* **2011**, *13*, 5815−5824.
(22) Panthani, M. G.; Akhavan, V.; Goodfellow, B.; Schmidtke, J. P.; Dunn, L.; Dodabalapur, A.; Barbara, P. F.; Korgel, P. A. *J. Am. Chem. Soc.* **2008**, *130*, 16770−16777.
(23) Zhong, H.; Zhou, Y.; Ye, M.; He, Y.; Ye, J.; He, C.; Yang, C.; Li, Y. *Chem. Mater.* **2008**, *20*, 6434−6443.
(24) Xia, C.; Cao, L.; Liu, W.; Su, G.; Gao, R.; Qu, H.; Shi, L.; He, G. *CrystEngComm* **2014**, *16*, 7469−7477.
(25) Lu, X.; Zhuang, Z.; Peng, Q.; Li, Y. *CrystEngComm* **2011**, *13*, 4040−4045.
(26) Beberwyck, B. J.; Surendranath, Y.; Alivisatos, A. P. *J. Phys. Chem. C* **2013**, *117*, 19759−19770.
(27) Son, D. H.; Hughes, S. M.; Yin, Y.; Alivisatos, A. P. *Science* **2004**, *306*, 1009−1012.
(28) van der Stam, W.; Gantapara, A. P.; Akkerman, Q. A.; Soligno, G.; Meeldijk, J. D.; van Roij, R.; Dijkstra, M.; de Mello Donega, C. *Nano Lett.* **2014**, *14*, 1032−1037.
(29) Li, H.; Zanella, M.; Genovese, A.; Povia, M.; Falqui, A.; Giannini, C.; Manna, L. *Nano Lett.* **2011**, *11*, 4964−4970.
(30) van der Stam, W.; Akkerman, Q. A.; Ke, X.; van Huis, M. A.; Bals, S.; de Mello Donega, C. *Chem. Mater.* **2014**, DOI: 10.1021/cm503929q.
(31) Luther, J. M.; Zheng, H.; Sadtler, B.; Alivisatos, A. P. *J. Am. Chem. Soc.* **2009**, *131*, 16851−16857.
(32) Bryks, W.; Wette, M.; Velez, N.; Hsu, S.-W.; Tao, A. R. *J. Am. Chem. Soc.* **2014**, *136*, 6175−6178.
(33) Li, W.; Shavel, A.; Guzman, R.; Rubio-Garcia, J.; Flox, C.; Fan, J.; Cadavid, D.; Ibáñez, M.; Arbiol, J.; Morante, J. R.; Cabot, A. *Chem. Commun.* **2011**, *47*, 10332−10334.
(34) Wang, Y.; Hu, Y.; Zhang, Q.; Ge, J.; Lu, Z.; Hou, Y.; Yin, Y. *Inorg. Chem.* **2010**, *49*, 6601−6608.
(35) Li, L.; Pandey, A.; Werder, D. J.; Khanal, B. P.; Pietryga, J. M.; Klimov, V. I. *J. Am. Chem. Soc.* **2011**, *133*, 1176−1179.
(36) Hovmöller, S. *Ultramicroscopy* **1992**, *41*, 121−135.
(37) Chen, B.; Zhong, H.; Zhang, W.; Tan, Z.; Li, Y.; Yu, C.; Zhai, T.; Bando, Y.; Yang, S.; Zou, B. *Adv. Funct. Mater.* **2012**, *22*, 2081−2088.
(38) De Trizio, L.; Prato, M.; Genovese, A.; Casu, A.; Povia, M.; Simonutti, R.; Alcocer, M. J. P.; D'Andrea, C.; Tassone, F.; Manna, L. *Chem. Mater.* **2012**, *24*, 2400−2406.
(39) Delerue, C.; Lannoo, M. *Nanostructures: Theory and Modeling*, 1st ed; Springer: New York, 2004.
(40) Donega, C.d. M.; Koole, R. *J. Phys. Chem. C* **2009**, *113*, 6511−6520.
(41) (a) JCPDS card R120113-9, low-chalcocite Cu_2S. (b) JCPDS card 01-077-9459, wurtzite $CuInS_2$. (c) JCPDS card 00-032-0456, β-In_2S_3.
(42) Rivest, J. B.; Jain, P. K. *Chem. Soc. Rev.* **2013**, *42*, 89−96.
(43) Groeneveld, E.; Witteman, L.; Lefferts, M.; Ke, X.; Bals, S.; van Tendeloo, G.; Donega, C. d. M. *ACS Nano* **2013**, *7*, 7913−7930.
(44) Pearson, R. G. *Inorg. Chem.* **1988**, *27*, 734−740.
(45) Xie, Y.; Riedinger, A.; Prato, M.; Casu, A.; Genovese, A.; Guardia, P.; Sottini, S.; Sangregorio, C.; Miszta, K.; Ghosh, S.; Pellegrino, T.; Manna, L. *J. Am. Chem. Soc.* **2013**, *135*, 17630−17637.
(46) Chakrabarti, D. J.; Laughlin, D. E. *Bull. Alloy Phase Diagrams* **1983**, *4*, 254−270.
(47) Noerby, P.; Johnsen, S.; Iversen, B. B. *ACS Nano* **2014**, *8*, 4295−4303.
(48) Buerger, M. J.; Wuensch, B. J. *Science* **1963**, *141*, 276−277.
(49) Evans, H. T. *Nature* **1971**, *232*, 69−70.
(50) Wyckoff, R. W. G. *Structure of Crystals*; American Chemical Society Monograph Series; American Chemical Society: Washington, DC, 1935.
(51) Diehl, R.; Nitsche, R. *J. Cryst. Growth* **1975**, *28*, 306−310.
(52) Huang, X.; Li, S.; Huang, Y.; Wu, S.; Zhou, X.; Li, S.; Gan, C. L.; Boey, F.; Mirkin, C. A.; Zhang, H. *Nat. Commun.* **2011**, *2*, 292.

DOI: 10.1021/cm504340h
Chem. Mater. 2015, 27, 621−628